

and cutting-edge seismic imaging technology. The data was processed through an advanced velocity modelling sequence with the PreSDM (pre-stack depth migration) of the final output extending to a depth of 20 km in order to enable modelling of deep crustal features. The dense coverage of gravity and magnetic data acquired alongside the 3D seismic data enabled production of a unique set of high-resolution anomaly maps for use in potential fields modelling. For example, shallow Albian carbonate rafts, Aptian salt walls and ponded Upper-Cretaceous mini-basins are clearly visible in the higher spatial frequencies of the gravity data (Figure 2) (Duval et al., 2015). The magnetic data contains information from a broad range of scales, with the dominant signal coming from the magnetic material in or near to the basement. In addition, enhancements of the magnetic data and 3D Euler depth estimates have clear correlations with features observed on the seismic sections, confirming the robustness and value of the data set.

Tectonic context

The study area is located on the West African margin of the central segment of the South Atlantic. The Central Atlantic rift started in Early Cretaceous (Berriasian) times as continental depositional conditions prevailed. The rifting phase culminated in Aptian times, accompanied by deposition of a thick salt layer, owing to the first sporadic sea incursions into the area, and cyclical evaporation phases. Shallow marine conditions dominated throughout the margin during Albian times, when a thick carbonate shelf was formed as Africa started to drift away from America. Thereafter, in a predominantly deep-water, open marine depositional environment, the Upper Cretaceous and Tertiary formations were mainly composed of siliciclastic sediments with mudstones, sandstone and occasional limestone beds.

A broad variety of plate tectonic models describing the context and development of the Gabon South Basin has been published by different research teams. Most of these studies and descriptions converge towards a simple-shear model, ranging from a pure lower-plate extensional margin (Clerc et al., 2017) to a lower-plate margin with a local transitional upper-plate margin (Lister et al., 1986) separated by a number of transfer zones in the area (Peron-Pinvidic et al., 2015). Although the Gabon South Basin has generally been described as a non-volcanic passive margin, there is still doubt around this. For example, it has been classified as ‘indefinite/uncertain’ in Reston’s ‘magma-poor’ vs. ‘magma-dominated’ margin classification (Reston, 2009).

In summary, the north-eastern half of the study area lies on continental crust and the south-western corner lies on oceanic crust. In between, we find the continent-ocean transition zone (COTZ) on a NW-SE trend which typically evolves from stretched, thinned continental crust, to possibly-intruded

continental crust or even exhumed mantle, and then ultimately oceanic crust. The characterization of these processes and the nature of the transition in and around the COTZ is the main focus of this article. The kinematic complexity of the South Atlantic opening suggests several extensional stages with slight changes in their stress orientations. Literature suggests (Granot and Dymant, 2015; Eagles and Perez-Diaz, 2017) that this scenario becomes exacerbated with long transform faults, such as in the Atlantic rift case, with the possibility of a mixed exhumed mantle adjacent to areas with densely intruded thinned crust. The gravity, magnetic and seismic datasets were analysed and interpreted in accordance with current theories of the tectonic setting, but new ideas, complementary information and developments were also considered to build a more detailed picture of the tectonic history of this basin.

Seismic evidence

The structures revealed by 3D regional seismic dip-lines, support a simple-shear, lower-plate margin model with a relatively shallow detachment (~10 km sub-sea and 6-7 km

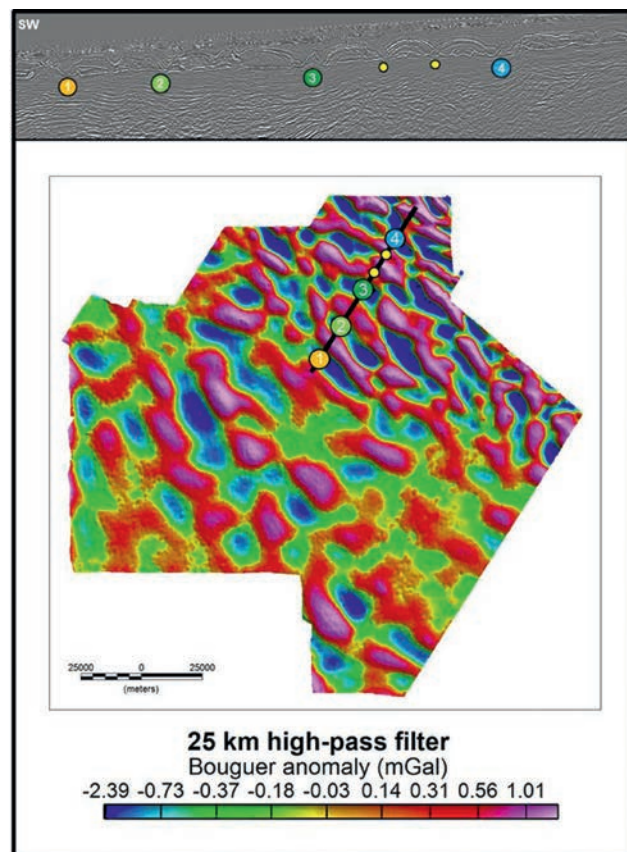


Figure 2 Correlation between seismic and 25km high-pass filter of the Bouguer anomaly map.

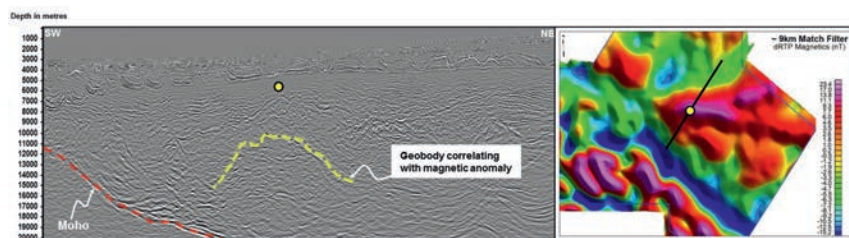


Figure 3 Correlation of geobodies in the seismic with magnetic anomalies.

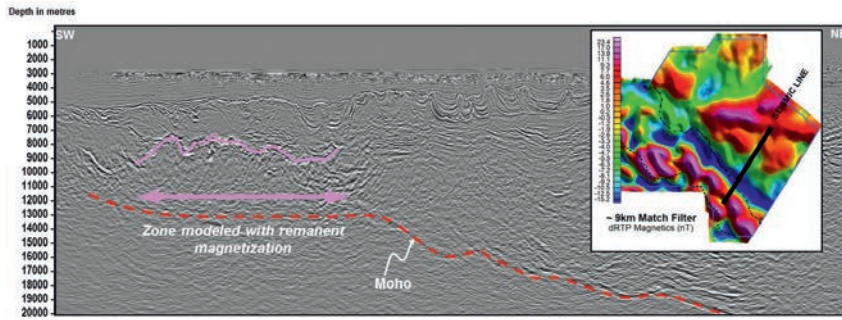


Figure 4 Seismic example of a zone modelled with remanent magnetization.

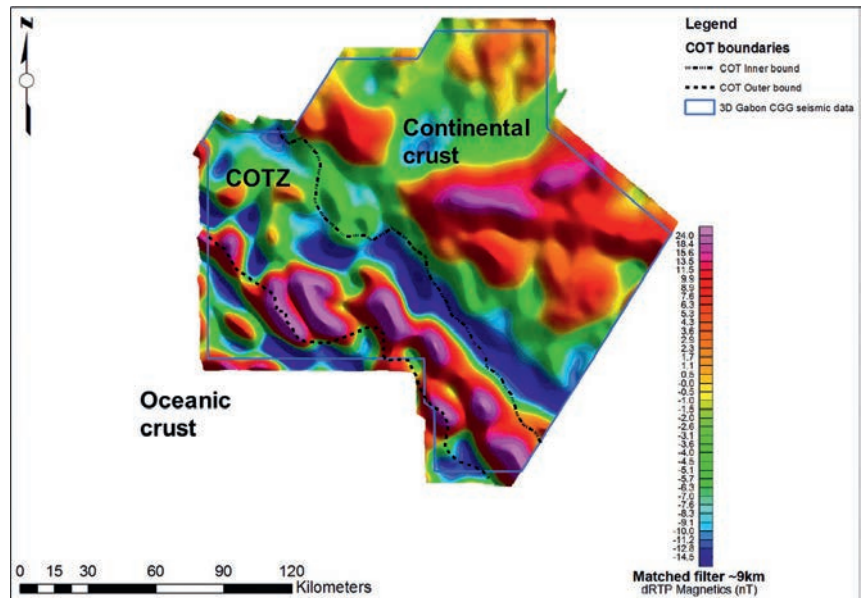


Figure 5 dRTP transformed magnetic anomaly map with the main tectonic domain interpreted over the area of study.

below seabed), converting into a large basin-scale fault flanking the northeast side of the basin in a NW-SE strike orientation and dipping towards the southwest. This detachment fault reaches a near-horizontal angle, underneath what is interpreted as hyper-extended continental crust, where the thickest section of post-rift sediments is recorded (Figure 3 and 4). North east of that fault, the seismic clearly images large syn-rift rotated fault blocks with visible syn-kinematic sediment growth, while the deep seismic grain becomes a lot more chaotic towards the south west beyond the detachment fault. According to Reston (2009), the development of this major detachment fault can be related to areas of possible serpentinization of the upper mantle. On CGG's seismic data, a continuous deep crustal reflector, interpreted as Moho, rises from a depth greater than 20 km to the north-east to reach as shallow as 8-9 km in places where the detachment fault becomes horizontal.

Another important feature observed in the seismic data, is the presence of strong, localized reflectors at depths that most probably relate to volcanic intrusions. These seem to have intruded sediments all the way up to the Aptian-Albian section around the south-west edge of the COTZ (Figure 5). However, there is no evidence of extrusive volcanic materials such as Seaward Dipping Reflectors on the seismic data.

Hence, for the Gabon margin we find it more appropriate to use the term 'magma-poor' (Sawyer et al., 2007 and Reston, 2009) rather than 'non-volcanic' margin. This leads to a more

suitable label for the study area as a magma-poor, locally hyper-extended, lower-plate margin.

Qualitative interpretation of potential fields maps

High resolution marine gravity and magnetic data were analysed alongside the large, regional, public domain data compilations. The marine gravity and magnetic maps show detailed, smaller-scale features and trends, which were compared to regional trends seen in the EMAG2 version 3 (Meyer et al., 2016) magnetic compilation and Sandwell Smith v23.1 gravity compilation (Sandwell et al., 2014). The Sandwell Smith gravity data was also used for padding the data in the 3D model.

The Bouguer anomaly of the marine gravity (with a reduction density of 2 g/cc) was used for the enhanced maps illustrated in Figure 2. The Bouguer anomaly attempts to remove the effect of the water/sediment density contrast. High-pass and match filters of the Bouguer gravity data show distinct anomalies in the shallower zones of the area of interest, and these correlate to gravity-sliding deformations (sediment mini-basins, salt walls and rafts, Figure 2) rather than deep tectonic features.

With appropriate filtering of the shorter-wavelength anomalies, the larger-scale anomalies show a good correlation with structures in the crust on seismic data. Modelling the data is the best way to separate the responses from the shallower salt/carbonate contrasts and those of deeper sediments and crustal

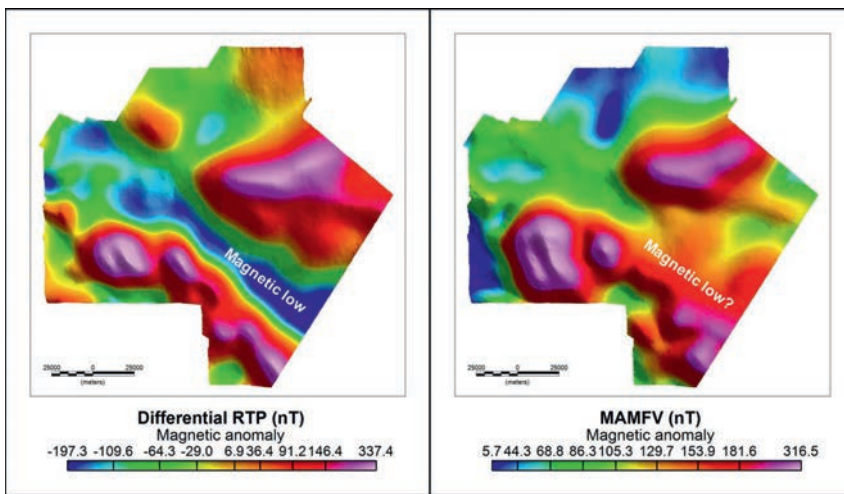


Figure 6 Comparison of magnetic field transformations.

contrasts. The density contrast at the Moho has a strong effect on the gravity response which is also evident in the main background trend of the Bouguer anomaly map.

A differential reduction to pole (dRTP) transformation was performed on the marine magnetic data. The dRTP technique (Arkani-Hamed, 1988) allows a range of inclination and declinations in the local magnetic field orientation, which is an important advantage when applying the transformation over a large area. Since there is the possibility of remanent magnetization, additional transformations were performed which are less sensitive to an assumed magnetic field orientation. These transformations include the magnitude of the anomalous magnetic field vector (MAMFV, Lourenco and Morrison, 1973), the normalized source strength (NSS, Clark, 2012) and the total gradient (TG, Nabighian, 1984).

A comparison of these grids showed good correlation with the standard dRTP in the northern areas. However, there was a poor correlation in the central southern area, where a broad magnetic low appears in the dRTP.

Figure 6 shows a comparison of the dRTP and the MAMFV. This suggests that the position of the dRTP results in the central southern area might not represent the true source location, and that near this area magnetic material was emplaced during an alternative magnetic field orientation.

The dRTP magnetic data was used for creating filtered maps, and results are considered more pertinent for the northern part of the area, where there is good correlation with the MAMFV and TG transformations. Derivative, band-pass and power spectrum analyses were performed, with one of the more interesting results being that of the band-pass filter for approximately 9 km depth of the dRTP (Figure 3). Magnetic lineations from this map correlate well with geobodies outlined in the seismic data.

There appear to be magnetized structures in the lower crust and deeper sediment section, suggesting zones of deep mafic intrusions and associated basement highs visible on seismic data.

In addition, we observe two distinct zones in the magnetic maps: The northwestern third of the survey area shows less magnetic field strength than the central and southeast areas. Interestingly, this division runs in an orientation similar to regional oceanic transfer faults. Upon additional examination of the EMAG2 version 3 dataset, offsets in the so-called ocean magnetic stripes, found south-west of the survey area, are aligned

on-trend with the boundary seen within the new marine magnetic data. This suggests that one regional fracture zone cuts through the northwestern side of the study area.

Joint seismic and potential fields modelling

As a first step, seismic interpretation was used to constrain the overburden and focus the potential fields modelling of the deeper crust. The density model for the sediment section was split into three sections: post Aptian-salt, salt and pre Aptian-salt. A probability density analysis was carried-out, cross-correlating velocity and density trends of the post-salt sediments from the available wells within the study area. Weighted linear regression of these probability density functions (PDFs) was used to estimate parameters for standard Gardner relationships. This was performed for each of the geological intervals interpreted in the logs and seismic data. The observed relationships were tabulated and used for density conversion of seismic tomographic velocities to populate a 3D density volume (voxel) for the sediments. For pre-salt sediments, dominated by the Dentale formation section, a linear relationship typical of compaction density curves was inferred from well data, with an upper limit of 2.65 g/cc. Salt was set to a constant 2.2 g/cc. Using this fixed structural framework and these density values, 3D models of the area were constructed and the gravity data were inverted to obtain quick estimates of depth-to- Moho and depth-to- crystalline basement.

In a second step, refined 2D and 3D geological models were produced. This was the opportunity to build several geological scenarios, initially tested on a selection of 2D lines, with the introduction of geobodies and other subdivisions of the geological model to compensate for anomalous potential fields signatures (Figure 7). This was accompanied by an improved understanding of the possible evolution of the basin so that 3D models were built to represent these scenarios accurately.

Importantly, the 2D models were built along dip-lines of the seismic data in order to limit any off-plane effects. The gravity and magnetic data were modelled together, in conjunction with seismic interpretation constraints. For the most part, the deep reflector interpreted as the Moho boundary was evident in the seismic sections, correlating very well with the Moho surface derived from inverted potential fields data in the first phase of

modelling, and indicated a sharp transition from 2.85g/cc above to 3.30g/cc below in terms of density contrast. Towards the onshore areas of the survey, the Moho boundary deepens below the 20-km limit of the depth-processed seismic data.

Furthermore, an additional horizon was interpreted from the seismic data in order to delineate the minimum depth of sediments. This horizon was picked to ensure that all data above the boundary had a 100% certainty of being sedimentary in nature, given the depositional patterns observed on the seismic. Using this as the upper limit of basement, the cross-sections were modelled to fit the gravity data. Magnetic depth estimates were used as guides for the edges of magnetic material, which could be magnetic basement, intrusions or intra-crustal features. The densities above basement were set to the sediment density voxel described above.

The basement was initially modelled with two layers: a lower ductile layer of higher density (2.85 g/cc), and an upper brittle layer of lower density (2.75 g/cc). This improved the fit of the modelled gravity response to actual measurements, and was also justified by variations observed in the compensative magnetic susceptibility values used in the model, and the magnetic depth estimates. Putting this into the context of the tectonic evolution of the area and crustal model scenarios, there were indications that exhumed mantle and deep mafic geobodies would need to be explained. The data interpretation also suggested possible zones

above the main crystalline basement where intrusives had formed dense meta-sediments.

During the 2D modelling phase of the project, the COTZ was better defined, and parts of this zone were modelled as having remanent magnetization. Remanent magnetization carries information about the timing and processes of emplacement of mafic materials as these rocks record the earth's magnetic field signature at the time they were formed (i.e. intensity and orientation). Keeping this in mind, it appears that the mafic materials in parts of the transition zone were emplaced at a time different from the magnetic materials in the continental crust to the north. Coincidentally, remanent magnetization was often modelled where the clear Moho reflection was lost on the seismic data (Figure 4). The magnitude of the remanent magnetization suggests large volumes of highly magnetic materials were emplaced. Our margin model implies that this may have occurred because of local hyperextension leading to extreme thinning with intrusion of brittle continental crust or possible mantle exhumation. The continental crust was modelled as two layers in the 2D models, i.e. lower and upper crust. As the continental crust thins towards the transition zone, our models show we preserve mainly the lower crust, hence confirming Peron-Pinvidic's 2015 model. With these geological scenarios modelled in 2D, the 3D model was initiated with the same boundaries. The minimum sediment depth horizon, interpreted from seismic data, was used as a boundary

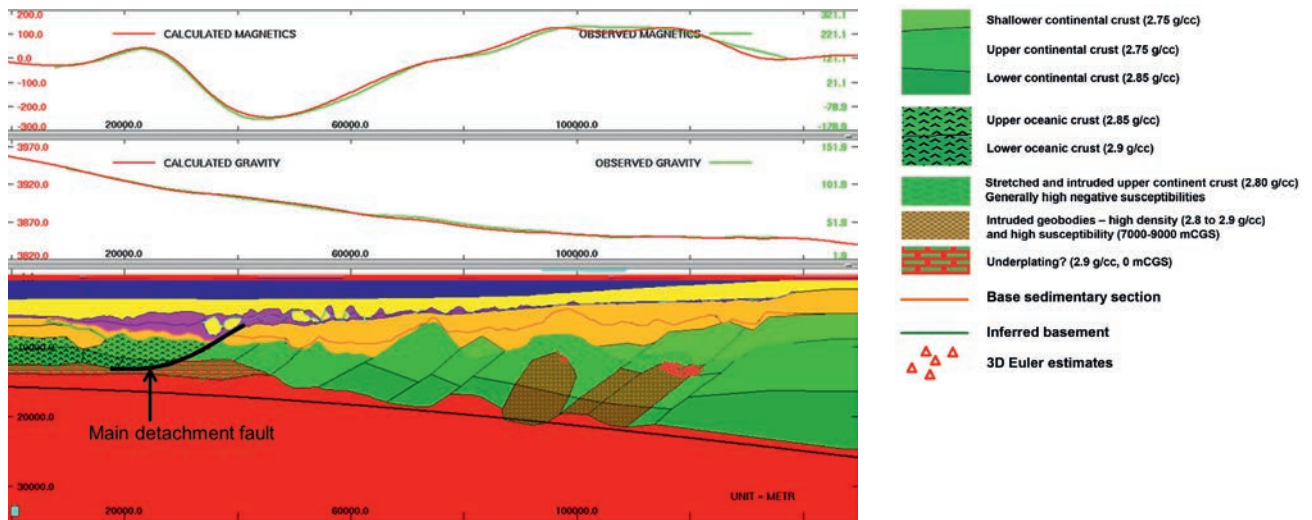


Figure 7 Example section of a combined gravity and magnetics model, testing various crust scenarios to fit the observed magnetics and gravity data.

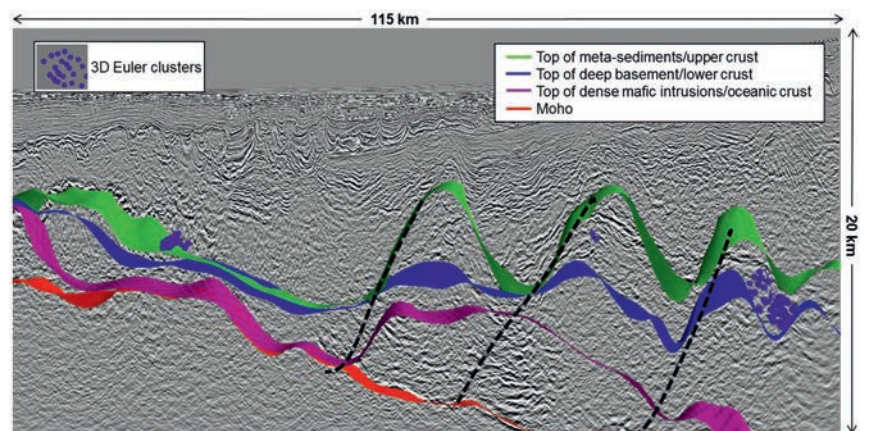


Figure 8 3D model layers of the deep crust overlain on seismic and their relationship with magnetic Euler depth estimates.

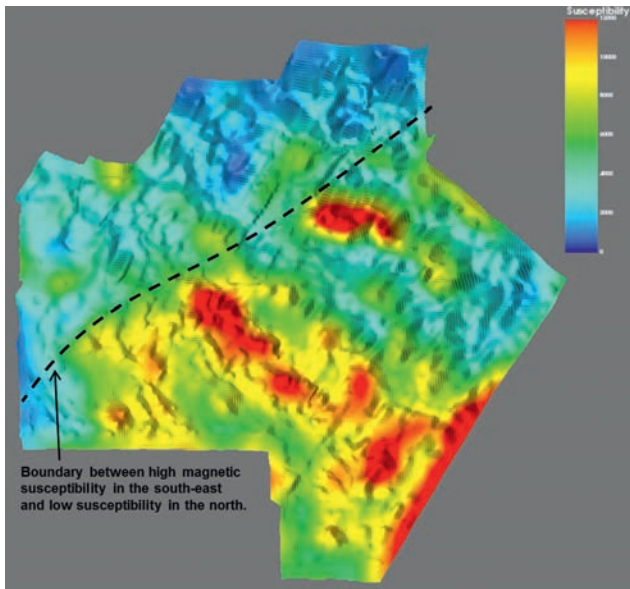


Figure 9 Susceptibility inversion targeting the lower sedimentary/upper basement zone and highlighting the possible presence of meta-sediments. Higher susceptibilities occur in the southeastern half of the area of study.

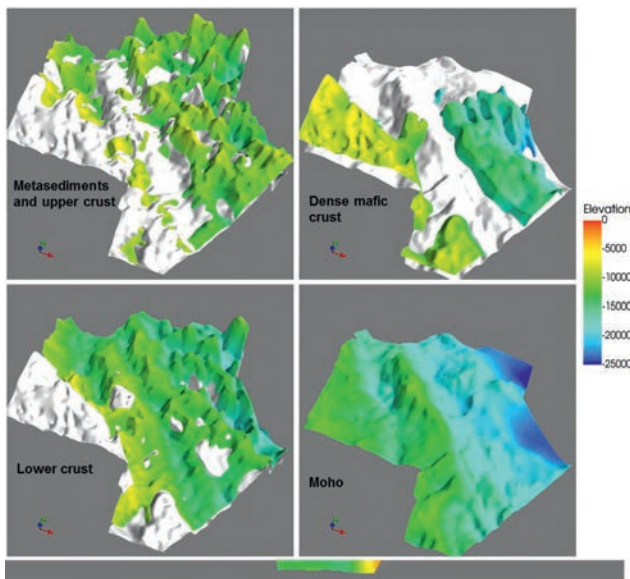


Figure 10 3D visualisation of the modelled deep crust layers.

for depth inversions of Top Basement. Again, the sediment density voxel derived from well data and seismic velocities was used for the sediment overburden. The crust was divided into three main density bodies: the meta-sediments/upper crust (2.75 g/cc), deep basement/lower crust (2.85 g/cc), and dense mafic intrusives or geobodies (2.9 g/cc). In the areas where oceanic crust was expected, the density of lower crust and mafic intrusives were also used to model the anticipated basalts and gabbros complex.

3D modelling was initially performed to fit the gravity data to a number of surface constraints from the seismic data, including the full sediment overburden interpretation, the minimum depth-to-basement horizon and the patches of visible Moho reflector. Within these constraints, the gravity data were inverted using the fixed density model defined previously, in order to generate 3D depth surfaces of the key crust features

described above. Good correlations were observed between the zones where mafic intrusions were expected from the magnetic, seismic and the plate tectonic model, and areas where upper crust or metamorphosed sediments were expected. For example, there were good correlations between the zones where dense intrusive geobodies were inverted and areas in the deep crust with clusters of high seismic amplitude reflectors (Figures 7 and 8). Areas of poorer correlation were iteratively adjusted by changing either the Moho surface or the quantitative properties of the model, such as density or magnetic susceptibility. The 3D model was regularly converted to ‘magnetic mode’, where the layers were assigned magnetic susceptibilities rather than densities. The susceptibilities were inverted in 3D for the layers where magnetic material would be expected, and the results viewed in conjunction with the seismic and gravity data.

Discussion

Although the seismic data shows great structural detail, understanding the creation of these structures and their relationship to petroleum prospectivity requires integration of all the data available. By combining the seismic data with the potential fields, well and geological data, interesting insights into the tectonic processes were obtained.

Beneath the salt, there appear to be sedimentary structures visible in the seismic to depths as great as 15 km in some areas. Some of these sedimentary layers have higher seismic amplitudes, and may in fact be layers of igneous material interlaid with sediments. Should some of these sedimentary packages contain mafic material, they could have a magnetic signal and would be of higher density. Contact metamorphism, or simply highly pressurized sediments, would also result in higher densities. When modelling the gravity, higher densities were required in many areas where the seismic signature suggests altered sediments or meta-sediments. These areas were often associated with clusters of 3D Euler magnetic depth estimates (Figure 8). The linear magnetic anomalies seen on the 9-km match filter of the dRTP magnetic data are coincident with some of the zones where more dense material is required (Figures 3, 4 and 7). The modelled high-density mafic material in the lower crust aligns in structurally coherent orientations as a result of mafic intrusions during periods of extension. Similarly, seismic sections overlain with the modelled layers may suggest that the meta-sediments and mafic material in the mid-section are related to mafic material moving up through deep crustal extensional faults (Figure 7 and 8).

An inversion for magnetic susceptibility was performed between the base of the sediments and the Moho (Figure 9). The areas of higher magnetic susceptibility suggest zones with a high concentration of mafic material. The presence of strong magnetic signatures on the southeastern side could be the result of more mantle material entering the crust, cooling and acquiring a magnetic susceptibility. The correlation of geobodies in the seismic in the mid-crust with anomalous high values in the magnetic data supports this theory (Figure 3, 7, 8 and 9). The orientation of these magnetic anomalies and geobodies could be explained as areas where faulting occurred in response to extensional strain prior to the opening of the Atlantic. It is more difficult to explain

the absence of strong magnetic anomalies on the northwestern side. While there is evidence of some mafic intrusions on this side, particularly in the areas of oceanic and transitional crust, the linear magnetic anomalies of the southeastern side do not occur in the continental crust farther north. While this part of the crust extends farther oceanward than the continental crust to the southeast, there appears to be less intrusion of magmatic material in the lower crust, and more ductile bowing of the mantle. Since the continental crust is farther oceanward, in the northwestern portion of the study area there may have been less strain than in the south, because of the counterclockwise separation of Africa from South America. This additional strain in the south may have sufficiently faulted the crust prior to ocean spreading for mantle material to intrude.

The success of this modelling relies on the integration of the seismic data, gravity and magnetic data with input from both geologists and geophysicists. Some aspects would have been challenging to define without the contribution of specific types of geophysical data. For example, without the magnetic data, the meta-sedimentary feature in the eastern side of the area would have been difficult to differentiate from other structures near by. Similarly, the gravity data helped to confirm the existence of larger sedimentary basins bounded by more dense meta-sediments. The high-resolution seismic data is paramount in this study – providing both confidence in the models, and the details needed to identify the finer aspects of petroleum prospectivity, such as tilted sediment blocks, and potential source kitchens.

Testing these concepts in integrated 3D models (Figure 10) provides constraints for the petroleum geologists in determining the tectonic history and nature of the basin. From the work done to date, we have developed a model that suggests that the study area is primarily composed of continental crust, with oceanic crust on the southwestern edge. A transition zone, with a width ranging from approximately 25 to 60 km, where continental crust is highly attenuated and intruded in some areas, separates the purely continental zone from the oceanic crust. The study did not reveal evidence of any extrusive volcanics on this margin but it is likely that there are intrusions at depth, where the crust is hyperextended. Owing to the high resolution of the input data, we have been able to infer more detailed tectonic processes occurring in the basin and locate them accurately, such as specific zones of extension, intrusions and fracture zones.

References

Arkani-Hamed, J. [1988]. Differential reduction-to-the-pole of regional magnetic anomalies. *Geophysics*, **53** (12), 1592-1600.

- Clark, D.A. [2012]. New methods for interpretation of magnetic vector and gradient tensor data I: eigenvector analysis and the normalised source strength. *Exploration Geophysics*, **43** (4), 267-282.
- Clerc, C., J-C Ringenbach, L. Jolivet and J-F Ballard [2017]. Rifted margins: Ductile deformation, boudinage, continentward-dipping normal faults and the role of the weak lower crust. *Gondwana Research*, (in press).
- Lourenco, J.S. and H. Frank Morrison [1973]. Vector magnetism anomalies derived from measurements of a single component of the field. *Geophysics*, **38** (2), 359-368.
- Meyer, B., R.Saltus and A. Chulliat [2016]. EMAG2: Earth Magnetic Anomaly Grid (2-arc-minute resolution) Version 3. National Centers for Environmental Information. NOAA, Model, doi:10.7289/V5H70CVX.
- Nabighian, M.N. [1984]. Toward a three-dimensional automatic interpretation of potential field data via generalized Hilbert transforms: Fundamental relations. *Geophysics*, **49** (6), 780-786.
- Lister, G.S., Etheridge, M.A. and Symonds, P.A. [1986]. Detachment faulting and the evolution of passive continental margins. *Geology*, **14** (3), 246-250.
- Péron-Pinvidic, G., Manatschal, G., Masini, E., Sutra, E., Flament, J.M., Hauptert, I. and Unternehr, P. [2015]. Unravelling the along-strike variability of the Angola-Gabon rifted margin: a mapping approach. *Geological Society, London, Special Publications*, **438**, 49-76.
- Reston, T.J. [2009]. The structure, evolution and symmetry of the magma-poor rifted margins of the North and Central Atlantic: A synthesis. *Tectonophysics*, **468**, 6-27.
- Sawyer, D.S., Coffin, M.F., Reston, T.J., Stock, J.M. and Hopper, J.R. [2007]. COBBOOM: The Continental Breakup and Birth of Oceans Mission. *Scientific Drilling*, **5**, 13-25.
- Sandwell, D.T., R.D. Müller, W.H.F. Smith, E. Garcia, R. Francis, [2014]. New global marine gravity model from CryoSat-2 and Jason-1 reveals buried tectonic structure. *Science*, **346** (6205), 65-67.
- Seton, M., Whittaker, J.M., Wessel, P., Müller, R.D., DeMets, C., Merkouriev, S., Cande, S., Gaina, C., Eagles, G., Granot, R., Stock, J., Wright, N., and Williams, S.E. [2014]. Community infrastructure and repository for marine magnetic identifications. *Geochemistry, Geophysics, Geosystems*, **15** (4), 1629-1641.
- Duval, G. and Firth, J. [2015]. G&G integration enhances acquisition of multi-client studies offshore Gabon. *World Oil*, July 2015 issue, 57-61.
- Granot, R. and Dymant, J., [2015]. The Cretaceous opening of the South Atlantic Ocean. *Earth and Planetary Science Letters*, **414**, 156-163
- Pérez-Díaz, L., and Eagles, G., [2017]. A new high-resolution seafloor age grid for the South Atlantic. *Geochemistry, Geophysics, Geosystems*. **18** (1), 457-470.